



## Thermodynamic, Electrochemical and Quantum Chemical Investigation of Thiomorpholin-4-ylmethyl-phosphonic Acid as Corrosion Inhibitor of Iron in Sulphuric Acid Solution

I. Elazhary<sup>1</sup>, H. Ben El Ayouchia<sup>2</sup>, M. R. Laamari<sup>1,\*</sup>, M. El Haddad<sup>1</sup>, S. Rafqah<sup>1</sup>,  
H. Anane<sup>2</sup>, M. L. Elidrissi Moubtassim<sup>2</sup>, S.-E. Stiriba<sup>2,3</sup>

<sup>1</sup>Equipe de Chimie Analytique et Environnement, Faculté Polydisciplinaire, Sidi Bouzid, B.P. 4162, 46 000 Safi Morocco.

<sup>2</sup>Equipe de Chimie Moléculaire Matériaux et Modélisation, Faculté Polydisciplinaire, Sidi Bouzid, B.P. 4162, 46000 Safi, Morocco.

<sup>3</sup>Instituto de Ciencia Molecular / ICMol, Universidad de Valencia, C/ Catedrático José Beltrán, 2, 46980, Valencia, Spain.

Received 05 Feb 2015, Revised 08 Oct 2015, Accepted 10 Oct 2015

\*Corresponding Author. E-mail : [r.laamari@uca.ac.ma](mailto:r.laamari@uca.ac.ma)

### Abstract

The inhibiting action of thiomorpholin-4-ylmethyl-phosphonic acid (TMPA) was investigated as the corrosion inhibitor of iron in 0.5M sulphuric acid (H<sub>2</sub>SO<sub>4</sub>) solution with the aid of potentiodynamic polarization test, electrochemical impedance spectroscopy (EIS) and weight loss measurements. The results revealed that thiomorpholin-4-ylmethyl-phosphonic acid (TMPA) is a good, mixed type inhibitor. The inhibition efficiency of TMPA on iron corrosion increases with increase in concentration of (H<sub>2</sub>SO<sub>4</sub>) and decreases with increase in temperature. The adsorption isotherm model of TMPA on the iron surface was in conformity with Langmuir isotherm model. Thermodynamic parameters were calculated and discussed. The local reactivity, analyzed by using Parr functions, shows that both sulphur and nitrogen atoms of TMPA are the main adsorption sites.

**Keywords:** iron; sulphuric acid; phosphonic acid; Inhibition, local reactivity.

### 1. Introduction

Organic inhibitors have attracted a large number of investigations as many industrial processes require protection of their facilities and equipment against corrosion [1]. Corrosion inhibitors are organic compounds with polar atoms such as N, S, P, O, unsaturated bonds and aromatic planar cycles, which have the ability to accept or donate electrons for adsorption onto the metallic surfaces by electrostatic interactions between the lone electron pair of the corrosion inhibitor and the valence electrons of the metal as well as interaction of  $\pi$ -electrons of the inhibitor with the metallic surface [2-5]. The inhibition efficiency increases in the order O<N<S<P [6].

Phosphonates are molecules that contain one or more groups R-PO(OH)<sub>2</sub>. Their good chemical stability and solubility in water enable their applications in oil production, formulation of detergents, as well as in the inhibition of corrosion and scale formation [7]. Among all these properties, their ability to form strong complexes with metals plays a major role in the fate and rate of transports of these compounds in the environment. Phosphonates constitute a group of chelating agents that are employed in cooling water and desalination systems to inhibit scale formation and corrosion, in the textile industry to stabilize peroxide-based bleaching agents, in industrial and house hold detergent formulations as chelating agents, and in nuclear medicine as bone-seeking carriers for radio nuclides [8].

The use of phosphonic acids to protect iron and iron alloy against corrosion has been the subject of various works [9-20]. Herein, we report on the inhibiting effect of thiomorpholin-4-ylmethyl-phosphonic acid (TMPA) on iron corrosion in 0.5 M H<sub>2</sub>SO<sub>4</sub> solution. The molecular structure of the organic phosphonic acid employed in the present study, as corrosion inhibitors, is given in fig.1.

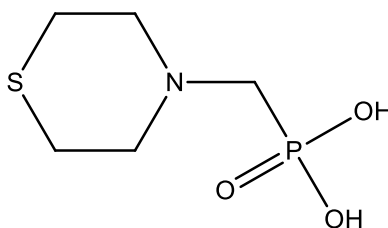


Figure 1. Structure of thiomorpholin-4-ylmethyl-phosphonic acid (TMPA)

## 2. Materials and methods

### 2.1. Inhibitor

Thiomorpholin-4-ylmethyl-phosphonic acid (TMPA) was synthesized, as described elsewhere, under microwave irradiation by using a microwave mono-mode Prolabo Synthe wave 402 [14]. The structure and purity of the obtained TMPA was confirmed by both FT-IR,  $^1\text{H}$  and  $^{13}\text{C}$  NMR spectroscopy. FT-IR (KBr,  $\nu\text{ cm}^{-1}$ ): 1475 (C-H), 1115 (P=O), 1160 (C-N), 925-980 (P-OH).  $^1\text{H}$  NMR (300 MHz,  $\text{CDCl}_3$ ): 2,54 (t,  $\text{CH}_2\text{-S}$ ), 2,73 (t,  $\text{CH}_2\text{-N}$ ), 2,75 (s,  $\text{CH}_2\text{-P}$ ), 4,80 ppm (br, OH).  $^{13}\text{C}$  NMR (75 MHz,  $\text{CDCl}_3$ ): 28 ( $\text{CH}_2\text{-S}$ ), 61,9 ( $\text{CH}_2\text{-N}$ ), 62,9 ( $\text{CH}_2\text{-P}$ ).

### 2.2. Electrochemical cell

Electrochemical experiments were performed using a conventional three electrode cell assembly. The working electrode is an Armco iron rotating disk with surface area of  $1\text{ cm}^2$  with the following composition (O: 0.03%, Mn: 0.03%, N: 0.018%, S: 0.018%, C: 0.012%, P: 0.004%, Fe: 99.8%). It was abraded with different emery papers up to 1200 grade, washed thoroughly with double-distilled water, degreased with AR grade ethanol and acetone and dried at room temperature.

Saturated calomel electrode (SCE) was used as the reference electrode. All the measured potentials presented in the experimental work are referred to this electrode. The counter electrode was a platinum plate with a surface area of  $2\text{ cm}^2$ .

The  $\text{H}_2\text{SO}_4$  solutions of 0.5 M were prepared by dilution of analytical grade 98%  $\text{H}_2\text{SO}_4$  with distilled water. The inhibitor was added to the freshly prepared  $\text{H}_2\text{SO}_4$  in the concentration range of 0.1 – 5 mM.

### 2.2. Methods

#### 2.2.1. Gravimetric measurements

Gravimetric measurements were carried out in a double walled glass cell equipped with a thermostat-cooling condenser. The solution volume was 100 mL of 0.5 M  $\text{H}_2\text{SO}_4$  with and without addition of different concentrations of inhibitor. The iron specimens used have a rectangular form ( $2\text{ cm} \times 2\text{ cm} \times 0.05\text{ cm}$ ). The immersion time for the weight loss was 24 h at 298 K and 6 h at the other temperatures. After the corrosion test, the specimens of iron were carefully washed in double-distilled water, dried and then weighed. The rinse removed loose segments of the film of the corroded samples. Triplicate experiments were performed in each case and the mean value of the weight loss is reported. The mean corrosion rate as expressed in  $\text{mg cm}^{-2}\text{ h}^{-1}$  was calculated through weight loss. The inhibition efficiency (IE %) was determined by using the following equation:

$$IE\% = \frac{CR_0 - CR}{CR_0} \times 100 \quad (1)$$

Where,  $CR$  and  $CR_0$  are the corrosion rates of iron with and without the inhibitor, respectively.

#### 2.2.2. Electrochemical measurements

Two electrochemical techniques, namely DC-Tafel slope and AC-electrochemical impedance spectroscopy (EIS), were used to study the corrosion behaviour of iron. All experiments were performed in one-compartment cell with three electrodes connected to a Voltalab 10 (Radiometer PGZ 100) system controlled by the Volta master 4 corrosion analysis software model.

Polarization curves were obtained by changing the electrode potential automatically from  $-800$  to  $-300$  mV versus open circuit potential ( $E_{\text{ocp}}$ ) at a scan rate of  $1\text{ mVs}^{-1}$ . The inhibition efficiency is calculated by the following equation:

$$IE\% = \frac{i_{corr}^0 - i_{corr}}{i_{corr}^0} \times 100 \quad (2)$$

where  $i_{corr}^0$  and  $i_{corr}$  are the corrosion current density values without and with inhibitor, respectively.

EIS measurements were carried out under potentiostatic conditions in the frequency range 100 - 0.01 Hz, with amplitude of 10 mV peak-to-peak, using AC signal at  $E_{ocp}$ . All experiments were performed after immersion for 60 min in 0.5 M  $H_2SO_4$  with and without addition of inhibitor. The inhibition efficiency obtained from the charge-transfer resistance is calculated by the following expression:

$$IE\% = \frac{R_t - R_t^0}{R_t} \times 100 \quad (3)$$

Where  $R_t$  and  $R_t^0$  are the charge-transfer resistance values with and without inhibitor, respectively.

The quantum chemistry calculations reported in this work have been performed at B3LYP/6-31G(+)(d,p) level of theory using the Gaussian 09 series of programs. We note that the cationic and anionic systems, required in the calculations of local indices were kept at the same geometry of the neutral system.

The electrophilic  $P_k^+$  and nucleophilic  $P_k^-$  Parr functions, were obtained through the analysis of the Mulliken ASD of the radical anion and the radical cation by single-point energy calculations over the optimized neutral geometries using the unrestricted UB3LYP formalism for radical species.

### 3. Results and discussion

#### 3.1. Weight loss measurements

##### 3.1.1. Effect of inhibitor concentration

Corroborative results between weight loss and other techniques have been reported [21-24]. The corrosion parameters obtained by conducting weight loss measurements for iron in the absence and presence of different concentration of TMPA in 0.5 M  $H_2SO_4$  are listed in Table 1.

**Table 1.** Corrosion parameters obtained from weight loss measurements for iron in 0.5 M  $H_2SO_4$  containing various concentrations of TMPA at 298 K.

C (M)	CR ( $mg\ cm^{-2}\ h^{-1}$ )	IE %
Blank	0.432	-
0.0001	0.220	49.1
0.0005	0.094	78.2
0.001	0.048	88.8
0.005	0.027	93.7

The data in Table 1 show that the corrosion rate values decrease as the concentrations of the inhibitor increase, i.e. the corrosion inhibition efficiency increases upon increasing the inhibitor concentration. This behavior is due to the adsorption and the coverage of inhibitor on iron surface [14,18-22]. To gain better understanding of thermodynamic properties of iron corrosion processes in the presence of TMPA, a detailed study on corrosion behaviour of iron was carried out at a temperature range 298–328 K using the weight loss technique.

##### 3.1.2. Effect of temperature

The temperature effect on the inhibited acid–metal reaction is quite complex because many changes occur on the metal surface such as rapid etching, inhibition, desorption and decomposition and/or rearrangement [25]. The values of corrosion rate and inhibition efficiencies for iron in 0.5 M  $H_2SO_4$  in the absence and presence of different concentrations of TMPA at various temperatures are summarized in Table 2. Fig. 2 shows the variation of the inhibition efficiency with TMPA concentrations between 298–328 K. The efficiency of the inhibition process increases by increasing the concentration of TMPA and goes over 93% at the concentration of 5 mM. Unsurprisingly, the inhibition efficiency decreases from 93.7% to 87.6% as the temperature is elevated from 298 to 328 K. This result suggests that physical adsorption is the predominant mechanism [26].

**Table 2.** Corrosion parameters obtained from weight loss for iron in 0.5 M H<sub>2</sub>SO<sub>4</sub> containing various concentrations of TMPA at different temperatures.

C (M)	CR (mg cm <sup>-2</sup> h <sup>-1</sup> )				IE %			
	298	308	318	328	298	308	318	328
Blank	0.432	0.82	1.3	2.25	-	-	-	-
0.0001	0.220	0.44	0.87	1.52	49.1	46.3	33.1	33.1
0.0005	0.094	0.22	0.44	0.75	78.2	73.1	66.1	68.1
0.001	0.048	0.092	0.212	0.435	88.9	88.8	83.7	82.5
0.005	0.027	0.062	0.122	0.321	93.7	92.4	90.6	87.6

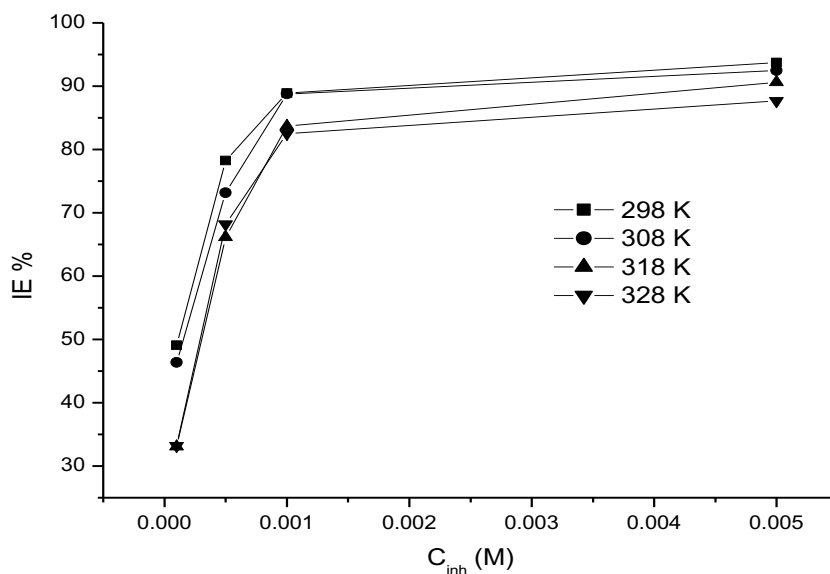


**Figure 2.** Variation of inhibition efficiency (IE%) in function of concentration of TMPA for iron in 0.5 M H<sub>2</sub>SO<sub>4</sub> at different temperatures.

Generally, the increase in temperature usually accelerates the hydrogen gas evolution in acidic medium, which results in higher dissolution rate of iron and mild steel. Thus, the increase in temperature led to the reduction of inhibitor adsorption and accelerates the dissolution process on metal surface. However, at higher concentration of TMPA, the increase in temperature has very little effect on inhibition efficiency. The constancy in efficiency of the inhibitor at higher concentration in the temperature range studied may be due to slight change in the nature of adsorption mode where the chemisorption alone or chemisorption accompanied by physisorption may occur [27].

### 3.1.3. Adsorption isotherm and thermodynamic consideration

Organic inhibitors were found to protect iron and mild steel from corrosion in acid medium by their adsorption on metal surface. In order to gain more information about mode of adsorption of TMPA on iron surface in 0.5 M H<sub>2</sub>SO<sub>4</sub> at different temperature, attempts were made to fit experimental data with several adsorption isotherms like Temkin, Langmuir, Freundlich, Frumkin, Bockris–Swinkels and Flory–Huggins isotherms. The best fit was obtained with Langmuir’s isotherm, which is in good agreement with Eq. (3).

$$\frac{C_{inh}}{\theta} = \frac{1}{K_{ads}} + C_{inh} \quad (4)$$

Where  $\theta$  is the surface coverage,  $C_{inh}$  is the molar concentration of inhibitor and  $K_{ads}$  is the equilibrium constant of the adsorption process.

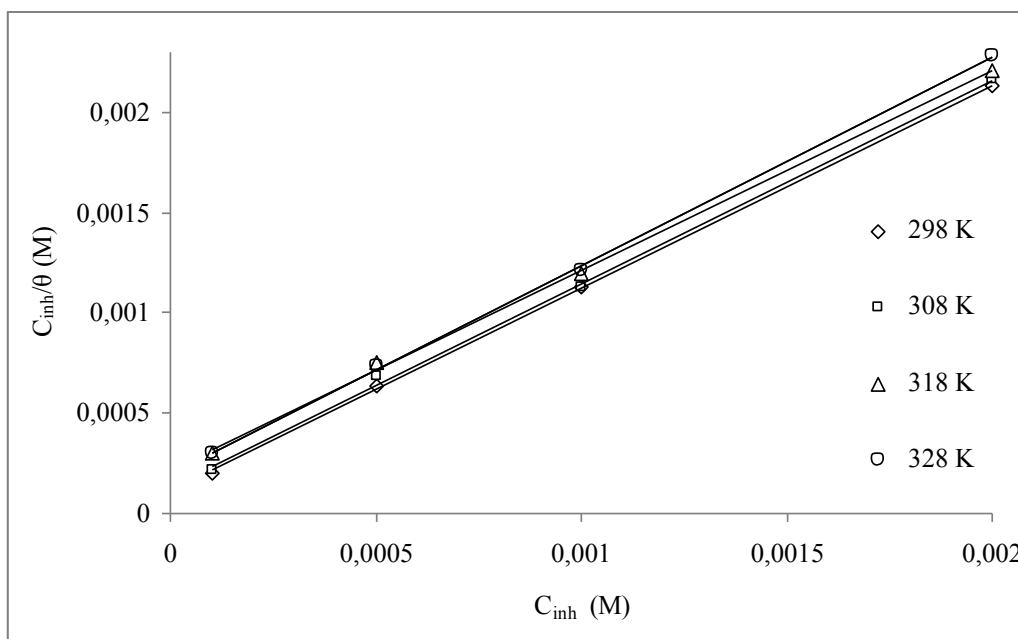


**Figure 3.** Langmuir’s isotherm adsorption model of TMPA on the iron surface in 0.5 M H<sub>2</sub>SO<sub>4</sub> at specific temperatures.

The plots of  $C_{inh}/\theta$  against  $C_{inh}$  were straight lines with almost unit slopes and are shown in Fig.3. It is found that all the regression coefficients are very close to 1 which indicates that the adsorption of TMPA on the iron surface obeys Langmuir adsorption isotherm.

The free energy of adsorption  $\Delta G^{\circ}_{ads}$ , also can be calculated using the following equation:

$$\Delta G^{\circ}_{ads} = -2.303RT \log(55.5K_{ads}) \quad (5)$$

where  $R$  is the universal gas constant,  $T$  the thermodynamic temperature and the value 55.5 is the molar concentration of water in the solution.

**Table 3.** Corrosion kinetic parameters for iron in 0.5 M H<sub>2</sub>SO<sub>4</sub> with and without different concentrations of TMPA.

Temperature (K)	R <sup>2</sup>	slope	K <sub>ads</sub> (M <sup>-1</sup> )	$\Delta G^{\circ}_{ads}$ (Kj mol <sup>-1</sup> )
298	0.999	1.01	10000	-32.80
308	0.998	1.01	9869	-33.86
318	0.998	0.99	5041	-33.18
328	0.999	1.03	4818	-34.10

The values of  $\Delta G^{\circ}_{ads}$  for the inhibitor on the surface of iron are given in Table 3. The negative values of  $\Delta G^{\circ}_{ads}$  indicate the stability of the adsorbed layer on the iron surface and spontaneity of the adsorption process.  $\Delta G^{\circ}_{ads}$  decrease to more negative values by increasing temperature, pointing to an endothermic process.

It is well known that values of  $\Delta G^{\circ}_{ads}$  around  $-20 \text{ kJ}\cdot\text{mol}^{-1}$  or lower are associated with the physisorption phenomenon where the electrostatic interaction assemble both the charged molecule and the charged metal, while those around  $-40 \text{ kJ}\cdot\text{mol}^{-1}$  or higher are associated with the chemisorption phenomenon where the sharing or transfer of organic molecules charge to the metal surface takes place [28, 29]. The calculated  $\Delta G^{\circ}_{ads}$  values were found to be between -34.10 and -32.8 kJ/mol, which prove that TMPA was physically adsorbed onto the iron surface. Moreover, the decrease in inhibition efficiency with increase in temperature may support the fact that the adsorption of TMPA on the metal surface is physical in nature. As the temperature increases, the number of adsorbed molecules decreases, leading to a decrease in the inhibition efficiency.

To obtain more details on the corrosion process, activation kinetic parameters such activation energy ( $E_a$ ); enthalpy ( $\Delta H^\circ$ ) and entropy ( $\Delta S^\circ$ ) were obtained from the effect of temperature using Arrhenius law (Eq. (5)) and the alternative formulation of Arrhenius equation (Eq. (6)) [30,31]:

$$\log(CR) = \log A - \frac{E_a}{2.303RT} \quad (6)$$

$$CR = \left(\frac{RT}{Nh}\right) \exp\left(\frac{\Delta S^\circ}{R}\right) \exp\left(-\frac{\Delta H^\circ}{RT}\right) \quad (7)$$

Where  $CR$  is the corrosion rate,  $R$  is the universal gas constant,  $T$  is the absolute temperature,  $A$  is the pre-exponential factor,  $h$  is Plank's constant and  $N$  is Avogadro's number.

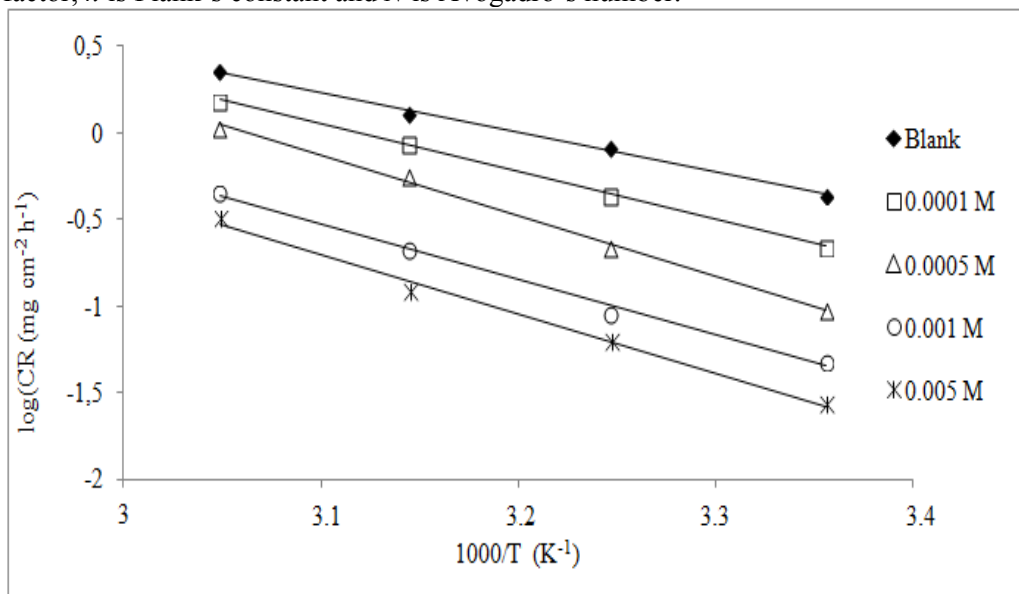


**Figure 4.** Arrhenius plots for iron corrosion rates (CR) in 0.5 M  $H_2SO_4$  with and without different concentrations of TMPA.

The plot of  $\log(CR)$  against  $1/T$  for iron corrosion in 0.5M  $H_2SO_4$  in the absence and presence of different concentrations of TMPA is presented in Fig.4. All parameters are given in Table 4.

**Table 4.** Thermodynamic parameters for the adsorption of TMPA on the iron in 0.5 M  $H_2SO_4$  at different temperatures.

C (M)	$E_a$ (KJ mol <sup>-1</sup> )	R	$\Delta H^\circ$ (KJ mol <sup>-1</sup> )	$\Delta S^\circ$ (JK <sup>-1</sup> mol <sup>-1</sup> )
Blank	44.04	0.997	41.44	-112.91
0.0001	52.74	0.999	50.14	-89.41
0.0005	56.78	0.997	64.18	-49.38
0.001	61.46	0.995	58.86	-73.39
0.005	65.80	0.992	63.15	-63.40

The calculated values of activation energies from the slopes are 44.04 and 65.80 kJ.mol<sup>-1</sup> for free acid and with the addition of 0.005 M of TMPA, respectively. It was observed that the activation energy increased in the presence of inhibitor. The higher  $E_a$  values, for inhibited solution than the uninhibited one indicate that a strong inhibitive action of the additives occurred with increasing energy barrier for the corrosion process. This emphasizes the electrostatic character of the inhibitor's adsorption on the metal surface [32].

Experimental corrosion rate values obtained from weight loss measurements was used to further gain insight on the change of enthalpy ( $\Delta H^\circ$ ) and entropy ( $\Delta S^\circ$ ) of activation for the formation of the activation complex in the transition state using equation (Eq. (6)).

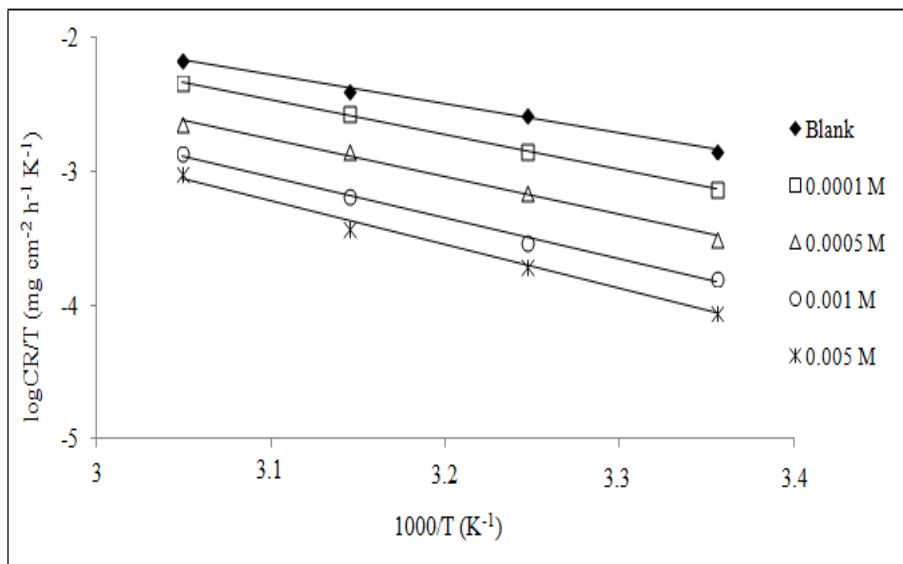


**Figure 5.** Transition-state plots for iron corrosion rates (CR) in 0.5 M H<sub>2</sub>SO<sub>4</sub> with and without different concentrations of TMPA.

Fig. 5 shows the plot of  $\log(CR/T)$  versus  $1/T$  for iron corrosion in 0.5 M H<sub>2</sub>SO<sub>4</sub> in the absence and presence of specific concentrations of TMPA. Straight lines were obtained with slope of  $(\Delta H^\circ/2.303R)$  and an intercept of  $[\log(R/Nh) (\Delta S^\circ/2.303R)]$  from which the values of  $\Delta H^\circ$  and  $\Delta S^\circ$  respectively were computed and listed also in Table 4, indicating that the positive signs of  $\Delta H^\circ$  both in the absence and presence of inhibitor reflects the endothermic nature of the iron dissolution process and suggesting that the dissolution process of iron is slower [33]. In addition, the entropy of activation ( $\Delta S^\circ$ ) in the absence and presence of TMPA has large and negative values. This indicates that the activated complex in the rate determining step represents an association rather than dissociation, which means that a decrease in disordering takes place on going from reactants to the activated complex [34,35].

### 3.2. Potentiodynamic polarization studies

**Table 5.** Polarization parameters and the corresponding inhibition efficiency of iron corrosion in 0.5 M H<sub>2</sub>SO<sub>4</sub> containing different concentrations of TMPA at 298 K.

$C_{inh}$ (M)	$E_{corr}$ (mV/SCE)	$i_{corr}$ ( $\mu A\ cm^{-2}$ )	$Ba$ (mV $dec^{-1}$ )	$Bc$ (mV $dec^{-1}$ )	EI %
blank	-504.8	425	59	-157.2	-
0.0001	-498	206	71.3	-138	51.5
0.0005	-488	82.9	65.3	-128	80.5
0.001	-488	48.2	65.1	-137	88.6
0.005	-480	27	64	-110	93.6

The potentiodynamic polarization behaviour of iron in 0.5 M H<sub>2</sub>SO<sub>4</sub> with the addition of various concentrations of TMPA is shown in Fig.6. The corrosion kinetic parameters such as corrosion potential ( $E_{corr}$ ), corrosion current density ( $I_{corr}$ ), anodic and cathodic Tafel slopes ( $Ba$  and  $Bc$ ) were derived from these curves and given in Table 5.

From the experimental data, it appears that the addition of the inhibitor decreases the dissolution rate of iron in acid media. From Table 5 it is clear that the corrosion current ( $I_{corr}$ ) value decreases from 425 to 27  $\mu A\ cm^{-2}$  with the addition of highest concentration of TMPA.

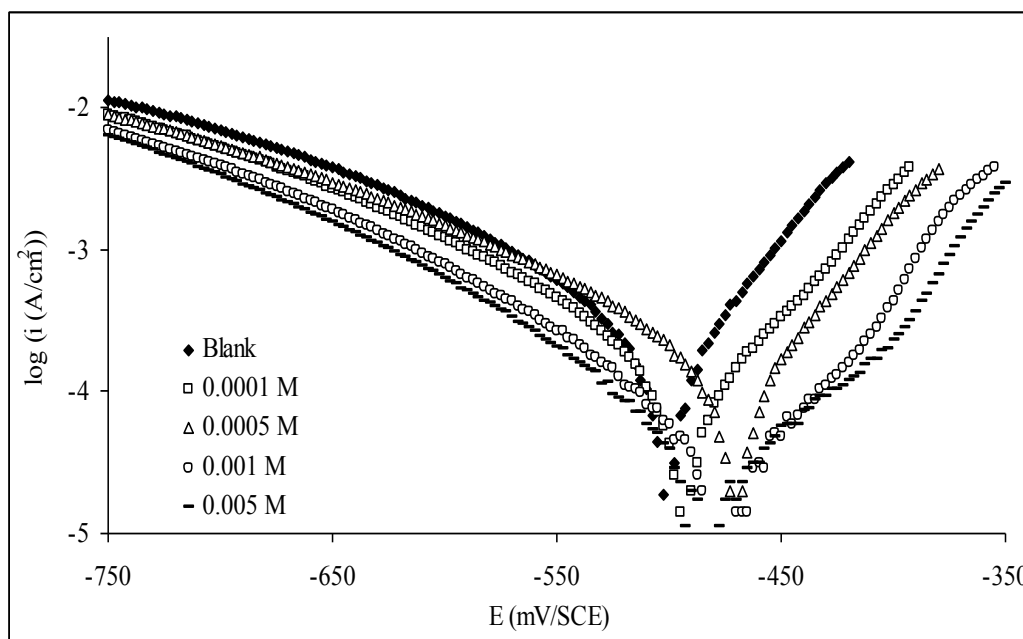
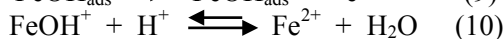
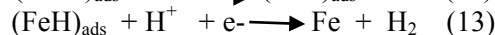
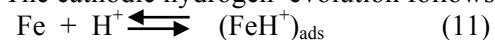


**Figure 6.** Potentiodynamic polarization curves for iron in 0.5 M H<sub>2</sub>SO<sub>4</sub> containing different concentrations of TMPA.

Data from Table 5 shows that cathodic and anodic Tafel slope values *B<sub>a</sub>* and *B<sub>c</sub>* are almost the same with and without inhibitor, which indicates that the inhibitor adsorbs on metal surface by simply blocking the active sites. The mechanism of anodic and cathodic reactions is not affected. A number of mechanistic studies on the anodic dissolution of Fe in acidic sulphate solutions have been undertaken, and the hydroxyl accelerated mechanism proposed initially by Bockris and Drazic [31] and reported by Oguzie [32] has gained overwhelming acceptance:



The cathodic hydrogen evolution follows:



This type of behaviour has been already observed for iron in acid solutions containing other inhibitors [20-32]. The addition of TMPA does not alter significantly the value of *E<sub>corr</sub>* indicating the mixed type of inhibiting behaviour of the added inhibitor.

### 3.3. Electrochemical impedance spectroscopy

Electrochemical impedance measurements were carried out the frequency range from 100 kHz to 0.1 Hz at open circuit potential. The Nyquist bode and phase angle representations of the impedance of iron in 0.5 M H<sub>2</sub>SO<sub>4</sub> with and without addition of various concentrations of TMPA are given in Fig. 7. The existence of single semi-circle shows that the single charge transfer process during the dissolution is unaffected by the presence of inhibitor molecules. Deviation of perfect circular shape is often referred to the frequency dispersion of interfacial impedance. This anomalous behaviour is generally attributed to the inhomogeneity of the metal surface arising from surface roughness or interfacial phenomena [36-38].

As shown in Fig. 7, Bode plots refer to the existence of an equivalent circuit that contains a single constant phase element in the metal/solution interface. According to appearance of phase angle plots (Fig. 7), increasing the concentration of TMPA in the test solution results in more negative values of the phase angle, which indicates superior inhibitive behavior due to adsorption of the metal surface of more TMPA molecules at higher concentrations [37-38].

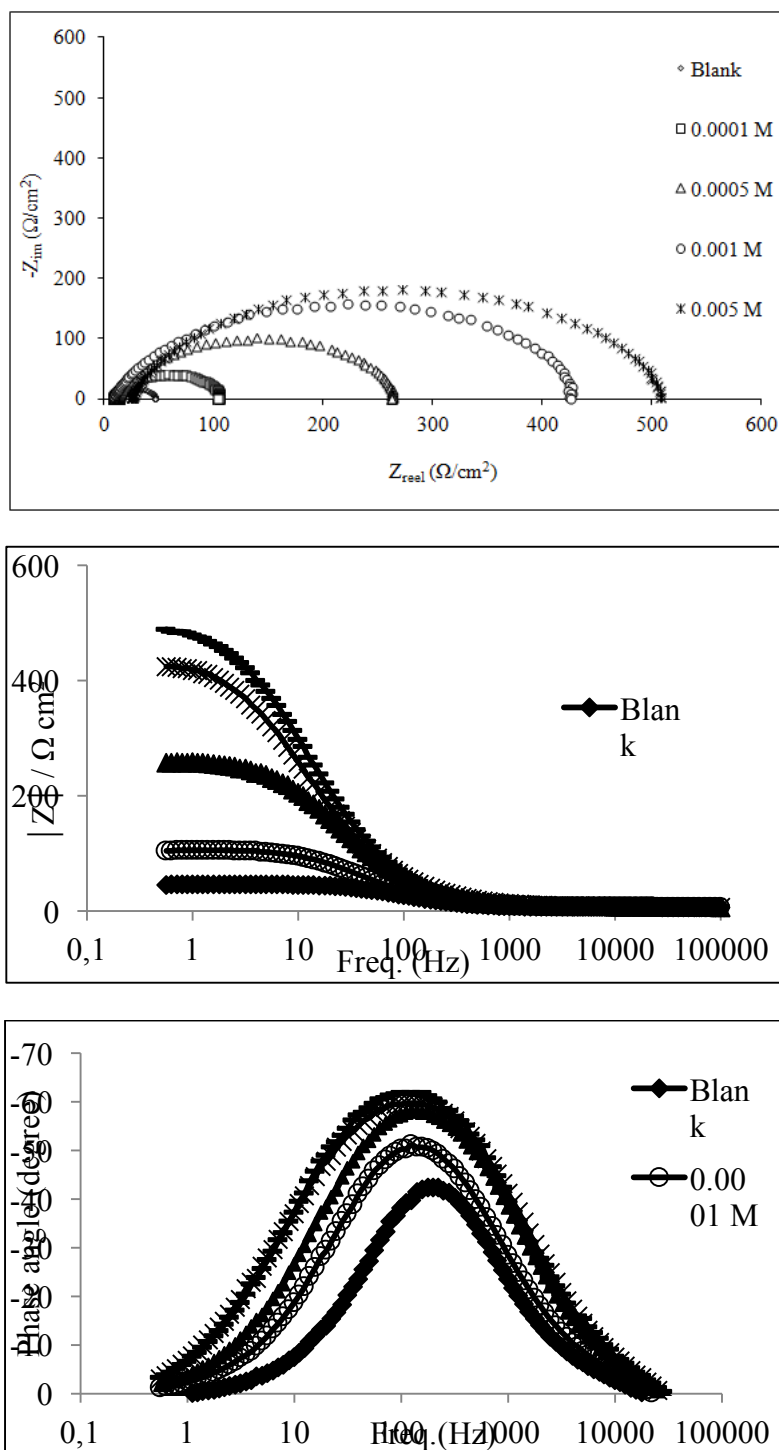


**Figure 7.** Nyquist, Bode and phase angle plots for iron in 0.5 M H<sub>2</sub>SO<sub>4</sub> with and without different concentrations of TMPA.

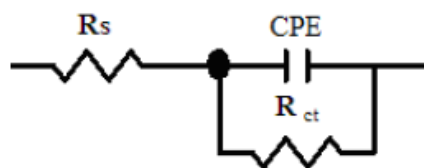


**Figure 8.** Equivalent circuit used to fit the obtained impedance spectra for iron in the absence and presence of the inhibitor.

The simplest fitting is represented by Randles equivalent circuit (Fig. 8), which is a parallel combination of the charge-transfer resistance ( $R_{ct}$ ) and a constant phase element CPE, both in series with the solution resistance ( $R_s$ ). The impedance of the CPE is expressed:

$$Z_{CPE} = \frac{1}{Y_0(j\omega)^n} \quad (14)$$

where  $Y_0$  is the magnitude of the CPE,  $n$  is the exponent (phase shift),  $\omega$  is the angular frequency and  $j$  is the imaginary unit. Depending upon the values of  $n$ , CPE may be resistive for  $n = 0$ , capacitance for  $n = 1$ , Warburg impedance for  $n = 0.5$  or an inductance for  $n = -1$ .

The charge transfer resistance ( $R_{ct}$ ) and the constant phase element CPE derived from these curves are given in Table 6. In fact, the addition of inhibitor increases the values of  $R_{ct}$  and reduces the CPE. The decrease in CPE is attributed to increase in thickness of electronic double layer [39]. The values of  $n$  obtained were close to unity that shows that the capacitive behavior of the interface. The increase in  $R_{ct}$  value is due to the formation of protective film on the metal/solution interface [39-42]. These observations suggest that TMPA molecules function by adsorption at metal surface thereby causing the decrease in CPE values and increase in  $R_{ct}$  values.

**Table 6.** Electrochemical impedance parameters of iron corrosion in 0.5 M  $H_2SO_4$  containing different concentrations of TMPA at 298 K.

$C_{inh}$ (M)	$R_s$ ( $\Omega\text{ cm}^2$ )	$C_{dc}$ ( $\mu\text{F}/\text{cm}^2$ )	$n$	$R_p$ ( $\Omega\text{ cm}^2$ )	EI%
blank	6	11	0.94	39	-
0.0001	7.1	9.83	0.86	101	61.4
0.0005	7.81	7.87	0.86	255	84.7
0.001	7.06	7,84	0.84	433	91
0.005	7.74	6.91	0.84	490	92

The data obtained from EIS technique are in good agreement with those obtained from potentiodynamic polarization and mass loss methods.

### 3.4. Quantum chemical studies

Density functional theory (DFT) is one of the most important theoretical models used in explaining the chemistry and physics of solids. A number of chemical concepts have been correlated within the framework of DFT [43]. The most fundamental parameter in DFT is the electron density  $\rho(r)$  based on which all the chemical quantities are expressed [44-45]. Since the theory is simpler than quantum mechanics, the interest has been grown in understanding the structure, properties, reactivity, and dynamics of atoms, molecules and clusters using DFT method. In the field of chemical reactions, DFT exceeds the limit of wave mechanics [46], and thus emerging as a unique approach for the study of reaction mechanism [47]. Recently, DFT has been used to analyze the characteristics of the inhibitor/surface mechanism and to describe the structural nature of the inhibitor on the corrosion process [48–50]. Furthermore, DFT is considered a very useful technique to probe the inhibitor/surface interaction. Quantum chemical calculation was employed using DFT to explain the experimental results obtained in this study and to further gain insight on the inhibition action of TMPA on the iron surface. In order to understand the electronic interaction between TMPA molecule with the metal surface, many theoretical parameters such as molecular orbital energies ( $E_{HOMO}$ ,  $E_{LUMO}$ ), energy gap ( $\Delta E$ ), dipole moment ( $\mu$ ), global hardness ( $\eta$ ) and the fraction of electrons transferred ( $\Delta N$ ) are useful to calculate [51-52].

The  $E_{HOMO}$  value is associated with the ability of the inhibitor molecule to donate electrons to the metal surface, therefore, higher  $E_{HOMO}$  values indicate easier donation of electrons from the corrosion inhibitor to the empty metal d orbitals. In contrast, the value of  $E_{LUMO}$  is related to the ability of the molecule to accept electrons, lower values of this property means that the inhibitor accommodates additional negative charge from the metal surface more easily. Consequently, the  $\Delta E$  ( $E_{HOMO}-E_{LUMO}$ ) gap is an important stability index. A lower HOMO–LUMO gap implies high stability for the molecule in the formed complex with the metal surface [53].

Table 7 shows the calculated quantum parameters for TMPA. The optimized equilibrium structure of TMPA is given in Fig. 8.

The data listed in Table 7 verify that TMPA has high value of  $E_{HOMO}$  and low value of  $E_{LUMO}$  with low energy band gap which supports its inhibition action on iron. Similar observations have been reported by Torres [54] on the adsorption properties of new synthesized thioureas derivatives on corrosion of mild steel in HCl solutions.

**Table 7.** Some molecular properties of TMPA using DFT at the B3LYP/6-31G+(d,p).

Quantum chemical parameters	$E_{HOMO}$ (eV)	$E_{LUMO}$ (eV)	$\Delta E$ (eV)	$\mu$ (Debye)	$\chi$ (eV)	$\eta$ (eV)	$\Delta N$ (e)
Value	-6.22	-0.52	5.7	2.066	3.37	2.85	0.63

The fraction of electrons transferred from the inhibitor molecule to the metallic atom ( $\Delta N$ ) was also calculated by us. We suggest that in the reaction of two systems with different electronegativities, namely metallic surface and an inhibitor molecule; the following mechanism will take place: the electron flow will happen from the molecule with the low electronegativity towards that of a higher value, until the chemical potentials are the same. In order to calculate the fraction of electrons transferred, a theoretical value for the electronegativity of bulk iron was used  $\chi_{Fe}=7\text{eV}$ , and a global hardness of  $\eta_{Fe}=0$ , by assuming that for a metallic bulk  $I = A$  because they are softer than the neutral metallic atoms. The calculations were performed using the following formula [55].

$$\Delta N = \frac{\chi_{Fe} - \chi_{inh}}{2(\eta_{Fe} - \eta_{inh})} \quad (15)$$

These quantities are related to electron affinity (A) and ionization potential (I), two useful parameters that help predicting a chemical behavior [56].

$$\chi = \frac{I + A}{2} \quad (16)$$

$$\eta = \frac{I - A}{2} \quad (17)$$

I and A are related in turn to  $E_{HOMO}$  and  $E_{LUMO}$  as follows:

$$I = -E_{HOMO} \quad (18)$$

$$A = -E_{LUMO} \quad (19)$$

The fraction of electrons transferred from inhibitor to the iron surface  $\Delta N$ , was calculated and listed also in Table 7. According to Lukovits, if  $\Delta N < 3.6$ , the inhibition efficiency increased by increasing electron donating ability at the metal surface [57]. In our case, the value of  $\Delta N$  for TMPA was lower than 3.6 which imply good ability of TMPA to donate its electrons to the iron surface. The Mulliken charge distribution of neutral and protonated TMPA is presented in Table 8.

**Table 8.** Mulliken charges for the neutral and protonated TMPA.

Atom	C1	C2	C3	C4	C5	N6	S7	P8	O9	O10	O11
Neutral	-0.205	-0.461	-0.485	-0.144	-0.532	-0.177	0.089	1.572	-0.709	-0.693	-0.704
protonated	-0.018	-0.507	-0.492	-0.099	-0.488	-0.609	0.217	1.617	-0.672	-0.694	-0.688

It has been reported that the more negative atomic charges of the adsorbed center, the more easily the atom donates its electron to the unoccupied orbital of the metal [56]. It could be readily observed that nitrogen, oxygen and carbon atoms have high charge densities. The regions of highest electron density are generally the sites to which electrophiles can attack [57]. Therefore, N, O and C were the active centers, which had the strongest ability of bonding to the metal surface. On the other hand, sulphur and phosphorus atoms carry positive charges, which are sites to which nucleophiles can attack. Therefore, TMPA can accept electrons from Fe through these atoms. Excellent corrosion inhibitors can not only donate electrons to unoccupied orbital of the metal, but also should accept free electrons from the metal. This property strengthens the chemisorption of TMPA on iron surface leading to a stable protective layer and thus retarding further corrosion of the metal in acid solution.

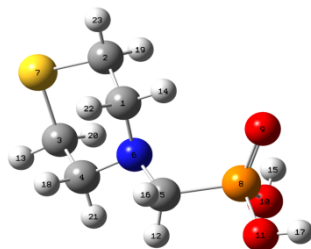


**Figure 9.** Optimized structure of thiomorpholin-4-ylmethyl-phosphonic acid (TMPA).

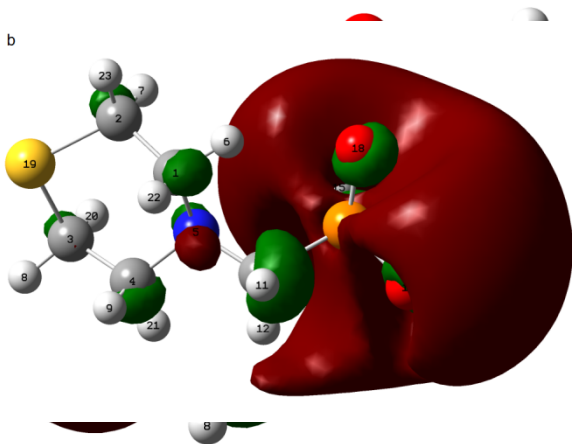


**Figure 10.** The highest occupied molecular orbital (HOMO) (a) and the lowest unoccupied molecular orbital (LUMO) (b) density of TMPA using DFT at the B3LYP/6-31G+(d,p).

Fig. 9 shows the distributions of the HOMO and LUMO orbitals computed at the B3LYP/6-31G+(d,p) level for the TMPA molecule. As expected, the HOMO orbitals are mainly located on the S and N atoms and the LUMO orbital is spread over O and P atoms. These results confirm the prediction that the reactive sites of TMPA are mainly located in sulphur and nitrogen atoms. Thus, the unoccupied d orbitals of Fe atom can accept electrons from inhibitor molecule to form coordinating bond and donate electrons by using its anti-bonding orbitals to form  $\pi$ -back-donating bond.

The local selectivity of the studied inhibitors is investigated using the Parr function  $P(r)$ , which is obtained from the analysis of the Mulliken atomic spin density (ASD) at the radical anion and at the radical cation of the corresponding reagents [58]. These local functions allow for the characterization of the most electrophilic and nucleophilic centers in a molecule, which is given by the following equations:

$$P^-(r) = \rho_s^{rc}(r) \quad \text{for electrophilic attacks} \quad (20)$$

$$P^+(r) = \rho_s^{ra}(r) \quad \text{for nucleophilic attacks} \quad (21)$$

Where  $\rho_s^{rc}(r)$  is the ASD of the radical cation, and  $\rho_s^{ra}(r)$  is the ASD of the radical anion. Each ASD condensed at the different atoms of the radical cation and the radical anion provides our local nucleophilic  $P_k^-$  and electrophilic  $P_k^+$  Parr functions of the neutral system. With these electrophilic and nucleophilic Parr functions at hand, we can redefine the local electrophilicity  $\omega_k$  and the local nucleophilicity  $N_k$  indices as follows:

$$\omega_k = \omega P_k^+ \quad (22)$$

$$N_k = N P_k^- \quad (23)$$

Using Parr's definition, we introduce the electrophilicity index  $\omega$ :

$$\omega = \frac{\mu^2}{2\eta} \quad (23)$$

Where  $\mu$  is the global chemical potential and  $\eta$  is the global chemical hardness. These quantities can be obtained in term of the one electron energies of the frontier molecular orbital (FMO) HOMO and LUMO,  $E_H$  and  $E_L$ , using the expressions:

$$\mu = \frac{(E_H + E_L)}{2} \quad (24)$$

$$\eta = (E_L - E_H) \quad (25)$$

Recently, Domingo has proposed for closed shell organic molecules, an empirical (relative) nucleophilic index  $N$  based on the HOMO energies  $E_{HOMO}$ , obtained within the Kohn–Sham scheme, [58-60] and defined as:

$$N = E_{HOMO}(Nu) - E_{HOMO}(TCE) \quad (20)$$

Tetracyanoethylene (TCE) is used as a reference in the nucleophilicity scale.

Table 9 shows the local nucleophilic  $P_k^-$  Parr functions of the cationic system and electrophilic  $P_k^+$  Parr functions of the anionic system and the local electrophilicity and nucleophilicity of the studied inhibitor.

**Table 9.** Prediction of reactive sites by using function Parr

Atom	C1	C2	C3	C4	C5	N6	S7	P8	O9	O10	O11
$P_k^-$	0.01	0.00	0.00	0.00	0.00	0.34	0.51	0.01	0.01	0.00	0.00
$P_k^+$	-0.266	-0.002	-0.311	-0.131	-0.868	0.159	0.362	2.573	-0.135	-0.264	-0.314
$N_k$	0.03	0.00	0.00	0.00	0.00	1.08	1.62	0.03	0.03	0.00	0.00
$\omega_k$	-	-	-	-	-	0.157	0.358	2.25	-	-	-

The calculated Parr functions are in good agreement with the results of the HOMO electron densities, indicating that the sulfur and nitrogen atoms have the highest value of  $N_k$  and  $\omega_k$ . This means that it would probably be the favorite sites for nucleophilic and electrophilic attacks. However the highest values of  $N_k$  of the sulphur atom and nitrogen atom, in comparison with the values of  $\omega_k$  imply that these sites will preferably react as electron donor than as electron acceptor. Moreover, the phosphorus atom has the highest value of  $\omega_k$ , which means that it would be the favorite site for electrophilic attack.

### 3.5. Mechanism of inhibition

As previously mentioned from weight loss analysis, potentiodynamic polarization and EIS measurements, the corrosion of Armco iron in 0.5 M  $H_2SO_4$  is retarded in the presence of different concentrations of TMPA. The results clearly show that the inhibition mechanism involves blocking of iron surface by inhibitor molecules via adsorption. The compound inhibits corrosion by controlling both the anodic and cathodic reactions. In acidic solutions the inhibitor exists as protonated species that adsorb on the cathodic sites of iron and decrease the evolution of hydrogen. The adsorption on anodic sites can occur either directly on the basis of donor-acceptor interactions between the electronic lone pair of nitrogen and sulfur atoms decreasing the anodic dissolution of Armco iron [42].

The present results are comparable and parallel with the literature findings. The difference in the inhibition efficiencies could be assigned to the different experimental conditions (corrosive media, temperature, etc.) and to the use of different metals or the same metal with different compositions. It was reported that piperidin-1-yl-phosphonic acid (PPA) is a good corrosion inhibitor of iron in 0.5 M  $H_2SO_4$  solution. [18] Weight loss measurements show that the inhibition efficiency depends on inhibitor concentration, and reaches 95% at optimum concentration. We have shown that hexamethylenediamine tetramethyl-phosphonic acid (HMDTMP) is a good corrosion inhibitor of carbon steel in acid solution. [15-17] Results obtained shows that the inhibition efficiency increases by the increase of concentration to attain 97% at  $5 \times 10^{-3}$  M. Bouklah et al. [61] studied the influence of [(2-pyridin-4-ylethyl)thio]acetic acid and pyridine on the corrosion inhibition of steel in sulphuric acid solution using weight loss, potentiodynamic polarisation and electrochemical impedance spectroscopy (EIS) measurements. The highest inhibition efficiency of 82% is observed at  $5 \times 10^{-3}$  M.

## 4. Conclusion

1. TMPA is an efficient inhibitor for iron corrosion in acidic medium displaying an inhibition efficiency that increases upon increasing its concentration but decreases upon rising the temperature.

2. The inhibition efficiencies obtained by polarization, EIS and weight loss measurements are in good agreement.
3. Polarization curves show that the inhibitor is a mixed type one.
4. The adsorption of TMPA on iron surface was found to be in accordance with Langmuir adsorption isotherm model. From the thermodynamic analysis point of view, the adsorption process is accompanied by a decrease in entropy of the system.
5. Theoretical calculations were in full agreement with the experimental results and show that the TMPA ability to donate electrons lead to its strong adsorption on metal surface.

## References

1. Granese S.L., Rosales B.M., Oviedo C., Zerbino J.O., *Corros. Sci.* 33 (1992) 1439.
2. Kaesche H., Hacherman N., *J. Electrochem. Soc.* 105 (1958) 191.
3. Blomgren B.E., Bockris J.O., *J. Phys. Chem.* 63 (1959) 1475.
4. Granese S.L., *Corros. Sci.* 44 (1987) 322.
5. Notoya T., *Corros. Eng. Jpn.* 27 (1978) 661.
6. Chetouani A., Hammouti B., Aouniti A., Benchat N., Benhadda T., *Progr. Org. Coat.* 45 (2002) 373.
7. Gledhill W.E., Feitjel T.C.J., in: Hutzinger O. (Ed.), *the Handbook of Environmental Chemistry*, Part F, vol. 3, Springer-Verlag, Berlin, 1992.
8. Nowack B., *Water Res.* 36 (2002) 4636.
9. Truc T.A., Pèbère N., Hang T.T.X., Hervaud Y., Boutevin B., *Corros. Sci.* 44 (2002) 2055.
10. Andijani I., Turgoose S., *Desalination* 123 (1999) 223.
11. Rajendran S., Reenkala S.M., Anthony N., Ramaraj R., *Corros. Sci.* 44 (2002) 2243.
12. Nakayama N., *Corros. Sci.* 42 (2000) 1897.
13. Gonzalez Y., Lafont M.C., Pebere N., Chatainier G., Roy J., Bouissou T., *Corros. Sci.* 37 (1995) 1823.
14. Amar H., Benzakour J., Derja A., Villemin D., Moreau B., Braisaz T., *Corros. Eng. Sci. Technol.* 41 (2006) 291.
15. Laamari M. R., Benzakour J., Berrekhis F., Abouelfida A., Derja A., Villemin D., *Arab. J. Chem.* 4 (2011) 271.
16. Laamari M. R., Benzakour J., Berrekhis F., Derja A., Villemin D., *Les Technologies de Laboratoire* 5 (2010) 18.
17. Laamari M. R., Benzakour J., Berrekhis F., Derja A., Villemin D., *Arab. J. Chem.*, doi: 10.1016/j.arabjc.2011.03.018 .
18. Laamari M. R., benzakour J., Berrekhis F., Bakasse M., Villemin D., *J. Mater. Environ. Sci.* 3 (2012) 485.
19. Laamari M. R., benzakour J., Berrekhis F., Bakasse M., Villemin D., *Arab. J. Chem.*, doi:10.1016/j.arabjc.2012.01.013.
20. Bouammali H., Hammouti B., Jama C., Bentiss F., Bekkouch K., Aouniti A., *Ind. Eng. Chem. Res.* 26 (2015) 2700276..
21. Prabakaran M., Vadivu K., Ramesh S., Periasamy V., *J. Mater. Environ. Sci.* 6 (2015) 2906-2916
22. Fouda A.S., Al-Sarawy A.A., El-Katori E.E., *Desalination* 201 (2006) 1.
23. Noor E.A., Al-Moubaraki A.H., *Mater. Chem. Phys.* 110 (2008) 145.
24. Fekry A.M., Mohamed R.R., *Electrochim. Acta* 55 (2010) 1933.
25. Kazarazi A., Kertit S., Aride J., Bougrin K., Soufiaoui M., *Bull. Electrochem.* 16 (2000) 97.
26. Lgaz H., Belkhaouda M., Larouj M., Salghi R., Jodeh S., Warad I., Oudda H., Chetouani A., *Mor. J. Chem.* 4 (2016) 101-111.
27. Zarrouk A., Zarrok H., Salghi R., Hammouti B., Bentiss F., Touir R., Bouachrine M., *J. Mater. Environ. Sci.* 4 (2013) 177-192
28. Khamis E., Bellucci F., Latanision R.M., El-Ashry E.S.H., *Corrosion* 47 (1991) 677.
29. Shukla S.K., Quraishi M.A., *Corros. Sci.* 51 (2009) 1007.
30. Singh A.K., Quraishi M.A., *Corros. Sci.* 52 (2010) 152.
31. Bockris J.O.M., Drazic D., *Electrochim. Acta* 7 (1962) 293.
32. Oguzie E.E., *Mater. Chem. Phys.* 87 (2004) 212.
33. Samkarapapaavinasam S., Ahmed M.F., *J. Appl. Electrochem.* 22 (1992) 390.

34. Andreani S., Znini M., Paolini J., Majidi L., Hammouti B., Costa J., Muselli A., *Int. J. Electrochem. Sci.*, 8 (2013) 11896.
35. Shih H., Mansfeld H., *Corros. Sci.* 29 (1989) 1235.
36. Martinez S., Metikos-Hukovic M., *J. Appl. Electrochem.* 33 (2003) 1137.
37. Elayyachy M., El Idrissi A., Hammouti B., *Corros. Sci.* 48 (2006) 2470.
38. Hosseini M.G., Ehteshamzadeh M., Shahrabi T., *Electrochim. Acta* 52 (2007) 3680.
39. Bentiss F., Traisnel M., Lagrenee M., *Corros. Sci.* 42 (2000) 127.
40. Murlidharan S., Phani K.L.N., Pitchumani S., Ravichandran S., *J. Electrochem. Soc.* 142 (1995) 1478.
41. Quraishi M.A., Rawat J., Ajmal M., *J. Appl. Electrochem.* 30 (2000) 745.
42. Chermette H., *J. Comput. Chem.* 20 (1999) 129.
43. Parr R.G., Yang W., *Density Functional Theory of Atoms and Molecules*, Oxford University Press, Oxford, 1989.
44. Jursic B.S., *J. Chem. Phys.* 104 (1996) 4151.
45. Parr R.G., Yang W., *J. Am. Chem. Soc.* 106 (1984) 4049.
46. Pearson R.G., *J. Am. Chem. Soc.* 85 (1963) 3533.
47. Lashkari M., Arshadi M.R., *J. Chem. Phys.* 299 (2004) 131.
48. Sein L.T., Wei Y., Jansen S.A., *Comput. Theor. Polym. Sci.* 11 (2001) 83.
49. Ebenso E.E., Arslan T., Kandemirli F., Caner N., Love I., *Int. J. Quant. Chem.* 110 (2010) 1003.
50. Ansari A., Znini M., Hamdani I., Majidi L., Bouyanzer A., Hammouti B., *J. Mater. Environ. Sci.* 5 (2014) 81-94
51. Gece G., Bilgiç S., *Corros. Sci.* 52 (2010) 3304.
52. Gao G., Liang C., *Electrochim. Acta* 52 (2007) 4554.
53. Saranya J., Sounthari P., Kiruthuka A., Parameswari K., Chitra S., *J. Mater. Environ. Sci.* 6 (2015) 425-444
54. Obot I. B., Obi-Egbedi N. O., Eseola A.O., *Ind. Eng. Chem. Res.* 50 (2011) 2098.
55. Musa A. Y., Kadhum A. H., Mohamad A. B., Takriff M. F., *Mater. Chem. Phys.* 129 (2011) 660.
56. Fu J., Li S., Wang Y., *J. Mater. Sci.* 45 (2010) 6255.
57. Belghiti M.E., Karzazi Y., Dafali A., Obot I. B., Ebenso E.E., Emran K. M., Bahadur I., Hammouti B., Bentiss F., *J. Mol. Liq.* 216 (2016) 874–886
58. Domingo L. R., Chamorro E. , Pérez P., *J. Org. Chem.*, 73 (2008) 4615.
59. Domingo L. R., Pérez P., *Org. Biomol. Chem.*, 9 (2011) 7168.
60. Kohn W., L. J. Sham, *Phys. Rev.*, 140 (1965) 1133.
61. Bouklah M., Attayibat A., Hammouti B., Ramdani A., Radi S., Benkaddour M., *Appl. Surf. Sci.* 240 (2005) 341.

(2016); <http://www.jmaterenvirosci.com>